JOURNAL OF ANCIENT HISTORY AND ARCHAEOLOGY

Institute of Archeology and Art History of
Romanian Academy Cluj-Napoca
Technical University Of Cluj-Napoca

Journal
of Ancient History and Archaeology

DOI: http://dx.doi.org/10.14795/j.v9i1

ISSN 2360 266x

ISSN–L 2360 266x

No. 9.1 /2022

CONTENTS

STUDIES

REVIEWS

Design & layout:
Petru Ureche

Studies

VIRTUAL ARCHAEOLOGY

INTEGRATED MULTI-ANALYTICAL STUDY OF THE BRONZE VESSEL FROM MĂLĂIEȘTI ROMAN FORT

Abstract: This paper presents an integrated multi-analytical documentation of a bronze vessel discovered in a 2nd century Roman military fort from ancient Dacia. The process involved 3D digitization, X-ray and hyperspectral imaging, and molecular, elemental, and structural analysis using Fourier Transform infrared spectroscopy, X-ray fluorescence, laser-induced breakdown spectroscopy and X-ray diffraction. The results of the study revealed the composition of the vessel metal and of the interior coating and the state of conservation through metal quality, internal cracks and corrosion compounds mapping. A 3D virtual reconstruction of the original aspect is also proposed based on the digitization and metal characterization results.
Keywords: *Roman bronze vessel, second century AD, Dacia Roman province, virtual archaeology, spectroscopy, X-ray imaging, hyperspectral imaging, military kitchenware.*

Laurențiu-Marian ANGHELUȚĂ
National Institute of Research and Development for Optoelectronics INOE 2000, Măgurele
laurentiu@inoe.ro

Ovidiu ȚENTEA
National Museum of Romanian History, Bucharest
ovidiu.tentea@gmail.com

Luminița GHERVASE
National Institute of Research and Development for Optoelectronics INOE 2000, Măgurele
ghervase@inoe.ro

Ioana Maria CORTEA
National Institute of Research and Development for Optoelectronics INOE 2000, Măgurele
ioana.cortea@inoe.ro

Monica DINU
National Institute of Research and Development for Optoelectronics INOE 2000, Măgurele
monica.dinu@inoe.ro

Lucian Cristian RATOIU
National Institute of Research and Development for Optoelectronics INOE 2000, Măgurele
lucian@inoe.ro

Anca Constantina PÂRĂU
National Institute of Research and Development for Optoelectronics INOE 2000, Măgurele
anca.parau@inoe.ro

Corresponding author address: ghervase@inoe.ro

DOI: 10.14795/j.v9i1.743
ISSN 2360 – 266X
ISSN–L 2360 – 266X

INTRODUCTION

Bronze is a large part of the archeometallurgical legacy of our ancestors. Mainly used for manufacturing jewelries, due to the similar aspect with gold[1], its ease of manufacturing and decoration made them suitable also for utility objects, such as tools, weapons, kitchenware. Amongst these, a distinct category is that of military vessels. This paper describes an integrated, comprehensive process of archaeometric documentation and virtual reconstruction of an artifact from this category: a 2nd century AD Roman bronze vessel (**Fig. 1**) that was recently discovered (2018), on the archaeological site of the "Roman fort of Mălăiești", Prahova County, Romania.

Considering the typical Roman vessels from the same period but also the size, shape and location of the object, it was assumed that this vessel was specific for military lifestyle (travelling, camping, and carrying). Although Roman military bronze vessels are not a rare archaeological find, and many studies have documented kitchenware objects in the Roman military life, only a few are focused on items with similar uncommon shape and dating from the same period. These are either dedicated to the archaeological and typology aspect of the vessel[2] or to the physico-chemical analysis of the alloy[3].

What captured the research team's interest for this item, was the archaeological context of the discovery which places it in a very precise time frame (101-118 A.D.), the unusual decoration for this type of object and the possibility of using a wide range of complementary methods within an

[1] FACSÁDY/VEREBES 2009.
[2] TUCKER 2012.
[3] KOTLAR *et alii* 2021.

Fig. 1. Photographic documentation of the bronze vessel: on site and after cleaning.

integrated approach. The shape of the vessel is uncommon from a typological point of view considering the repertoire of Roman bronze vessels produced during the 1st century A.D. In this regard, only one clear analogy has been identified so far: a bronze vessel from the Rijksmuseum van Oudheden, Leiden (The Netherlands). Unfortunately, there is no information related to the context of the discovery for this vessel, as it was dredged up from a river (Meuse) back in 1938. Archaeological literature would place this kind of vessels in a category with the Östland buckets (the Tingvoll or Westerwanna types). This broad category contains different types of Roman buckets, with different morphology, produced for a long period, between 1st century BC and 2nd century AD[4].

In this study, in support of the archaeological research, two main aspects were considered: an accurate 3D digitization followed by a virtual reconstruction of the vessel, and a thorough physico-chemical and imaging characterization of its conservation state. Photogrammetry was used for the 3D digitization, while the conservation state was assessed using: imaging techniques (X-ray digital radiographs[5] and hyperspectral image processing[6] and spectroscopy investigations: Fourier Transform infrared (FTIR) spectroscopy[7], X-ray fluorescence (XRF)[8], laser-induced breakdown spectroscopy (LIBS)[9] and X-ray diffraction (XRD)[10].

[4] KOSTER/RIEDERER 1997.
[5] CHELMUS/RADVAN/GHERVASE 2018; COSANO *et alii* 2018.
[6] LIANG 2011; GRAZZI *et alii* 2019.
[7] COSANO *et alii* 2018; KOTLAR *et alii* 2021.
[8] ANGELINI *et alii* 2004; ALBERGHINA *et alii* 2011; RUBIO-BARBERÁ *et alii* 2019.
[9] ALBERGHINA *et alii* 2011; NEVIN/SPOTO/ANGLOS 2012.
[10] UVAROV/POPOV/ROZENBERG 2015; AGRESTI *et alii* 2016.

Historical context of the Roman fort from Mălăiești (Prahova County, Romania)

The fort from Mălăiești is part of a small group of fortifications built by the Roman army north of Danube, during their conquest campaigns in Dacia. An important aspect regarding these fortifications is that their short-term functioning is well documented, giving the objects found within the site a precise dating. This fort was built during the advances of the Roman armies across the Carpathian Mountains to the present Transylvania region, starting with 101 A.D. and was functional until 118 A.D., the first year of the reign of emperor Hadrian, Trajan's successor[11]. The short-term functioning of this fort allows for a detailed reconstruction of a well-defined historical sequence, making this site a reference standard for the constructions and artefacts chronologically framed in the first years of the second century A.D[12].

The area of the fort was severely affected by agricultural leveling back in the 1980s, which made difficult the identification of the routes of the wooden walls and the distribution of the barracks buildings. The archaeological research (2011-2019) identified the burning level of the barracks, corresponding to the time when the garrison left. Based on this research it was concluded that the camp had 24 barracks, which means a considerable number of soldiers were hosted[13], possibly a full garrison for a *cohors militaria* or *ala quingenaria*, a unit between 600 and 800 soldiers[14]. The name of this troop remains unknown[16]. The correlation of the data gathered from geophysical measurements[15],

[11] ȚENTEA/MATEI-POPESCU 2015.
[12] ȚENTEA 2018.
[13] HODGSON/BIDWELL 2004.
[14] ȚENTEA/POPA/CÎMPEANU 2018.
[15] ȚENTEA/CĂLINA 2019.

regarding the camp plan, with those from the extensive excavations (~450 m^2) around a military barracks from the *sinister praetentura* revealed important information about the architecture and the internal structure of the building where the vessel was found.

The excavated barrack had 8 bedrooms (*contubernia*), with a usable area of about 12 m^2, doubled to the south by a corridor. The officer's residence (~ 80 m^2, divided into several rooms) was located at the eastern end of the barrack. A cellar was identified under the south-east room, located in the corner of the apartment. The vessel that is the subject of this paper was found in the cellar of this barrack along with several of its fragments (Supplementary material 1) and other objects with a significant number amphorae used for wine, olive oil and *garrum*[16], indicating their storage on wooden shelves and supports.

MATERIALS AND METHODS

The object. Archaeological discussion

The object was found partially damaged with a side wall bashed in and the base detached. It had some missing parts, of which several fragments were found nearby. The surface was covered with green, brown and black encrustation, due to corrosion processes.

The vessel has a globular body, with rounded shoulder, wide neck, and slightly inverted rim. It had flat base (now detached), made from a different metal sheet. From the point of view of the production process, the vessel was initially cast as a rough cylinder, which was subsequently hammered, in order to obtain the final shape. The body preserves a dotted decoration (possibly made by embossing), organized in two registers (as emphasized after 3D digitization: one towards the base, the other under the rim) divided by an undecorated strip on the shoulder. The remaining part of its neck presents only one metal loop, a band of the same material as the vessel, with a width 6.3 mm and 1 mm thickness, bended and rounded, with 8mm diameter, which suggests it had a handle of unknown design at some point, but now lost. The vessel has 15.6 cm height; 12 cm neck diameter; 18.7 cm maximum body diameter, 13.5 cm base diameter; thickness: between 1.77 mm (upper areas) and 2.33 mm (widest areas); 374 g (339 g the body + 35 g the bottom) weight.

Only two other vessels with similar decorations as the ones from Mălăiești and Leiden have been found in literature: an Östland bucket from the Netherlands, with a slightly different shape[17] and an ovoid bucket from France[18]. This can infer that such vessels were produced in a workshop which functioned in the provinces (in Gallia Belgica or Germania Inferior), most probably during the second half of the 1st century AD.

3D documentation

The subject was 3D digitized using photogrammetry, an image-based 3D digital reconstruction technique successfully applied in most cultural heritage digitization projects for some years[19] and based on the resulted 3D model a virtual reconstruction of the original shape was proposed. The virtual reconstruction was an important aspect due to the rarity of the vessel and thus the importance of sharing its hypothetical original form to other experts but also to the public.

3D Digitization using photogrammetry

The first step in this process was to make several important observations regarding the surface of the object. On the superior half of exterior surface, the metal had a polished aspect favoring significant specular reflections. This feature is problematic to both laser scanning and photogrammetry and usually results in loss of data, due to the specks of light reflection which occurs[20]. Another important aspect was that the object still had dirt layers on the interior (like a coating), so an accurate reconstruction of the interior metal surface would not have been possible. The real-life texture color needed for the final result and the complicated shape of the interior of the object were the deciding factors in favor of photogrammetry against other available methods.

In the data acquisition stage, the image set was recorded using the turntable method, following recommended procedures[21], with a 36-megapixel full frame professional camera (Nikon D810), with 35 mm lens and circular polarizing filter. An X-rite ColorChecker card was used for white balance and color corrections. A total of 214 selected images were used for processing.

The 3D reconstruction was realized with a specialized photogrammetric software, Agisoft Metashape (v 1.7). As the study requirements needed only the 3D mesh, the processing workflow implied image alignment followed by mesh generation using depth maps. 3D Mesh reconstruction used depth maps generated at *Ultra High* quality.

Virtual reconstruction

The virtual reconstruction of the object (Supplementary material 2) was based on the resulted photogrammetric 3D model. The purpose of this approach was to create a realistic shape and look of the object before it was damaged by time. Because of its rare shape and peculiar decorations, it posed great difficulty in establishing its original form. The main instrument used was Blender 3D v 2.9 software, with physical based rendering (PBR) materials to make the final render look as close to reality as possible.

Spectroscopic methods

The spectroscopic methods used in this study are non-invasive and nondestructive, with the exception of LIBS, which is micro-destructive. All the fragments found in the proximity of the vessel (Supplementary material 1), have been investigated using different methods, as follows.

Fourier transform infrared spectroscopy (FTIR) analysis

[16] OPAIȚ 2017.
[17] KOSTER/RIEDERER 1997.
[18] BARATTE *et alii* 1984.
[19] REMONDINO 2011.
[20] NICOLAE *et alii* 2014.
[21] ANGHELUTA 2019.

was carried out on corrosion products of various color and soil (sedimentary matrix), gently scratched from the surface of the samples using a scalpel and grinded in a mortar. FTIR was performed in attenuated total reflection (ATR) mode, using a SpectrumTwo FTIR spectrometer (PerkinElmer) equipped with a GladiATR accessory (monolithic diamond ATR crystal, Pike Technologies). Spectra were recorded by accumulating 32 scans at 4 cm^{-1} resolution in the 4000–380 cm^{-1} mid-infrared region. Spectra were baseline corrected. Data processing was done with Essential FTIR Spectroscopy Software Toolbox (Operant LLC).

X-ray fluorescence (XRF) spectroscopy was performed with portable hand-held TRACER III-SD energy-dispersive equipment (Bruker Elemental). Due to the surface morphology and shape of the vessel, XRF investigation was done on 9 fragments. For the largest samples, several spectra were acquired per sample, resulting a total of 15 spectra. The operating conditions were set at 40 kV, ~11 μA, 60 s acquisition time, using an Al and Ti filter to modulate the signal; the XRF analyzer' spot is ~ 3x4 mm.

Laser-induced breakdown spectroscopy (LIBS) was performed with a handheld spectrometer from SciAps that can operate in Argon purge environment, applied directly on the surface of interest. The equipment has a Q-switched Nd:YAG emitting at 1064 nm, with 5 mJ energy and 50 μm laser spot. It has a spectral range from 190 nm out to 950 nm, due to its 3 spectrometers. LIBS spectra were recorded for 100 pulses per each analyzed spot and the data were processed for the study of the chemical element distribution in stratigraphy.

X-ray diffraction (XRD) data were recorded on corrosion products from sample 7, using a SmartLab diffractometer (RIGAKU, Tokyo, Japan), equipped with 9kW Cu rotating anode and 5-axis vertical goniometer. The diffractometer was operated in parallel beam mode with high-resolution optics on the incident beam (2-bounces Ge(220) monochromator) to select Cu-Ka1 radiation (λ = 1.540597 Å). The measurements were performed in the range of 10-100° with a step size of 0.02°. Peak identification was made using the PDXL software data base.

Imaging techniques

X-Ray imaging. The X-Ray generator was Siefert Isovolt Mobile 160 with large focal spot of 5.5 mm and 91 cm working distance. The re-usable digital film detector was scanned with resolution of 35 μm per pixel and exported as JPEG files at 41.5 megapixels. This first exposure session was realized at high irradiation parameters (100 kV energy, 5 mA current intensity, 60 s exposure), in order to penetrate the thickness of the whole mass of soil and the metal vessel. A second exposure session (80 kV energy, 5 mA current intensity and 30 s exposure time) was done after the first cleaning and earth removal, to assess the conservation state of the object and find clues about the manufacturing technique, especially for the base and the exterior decorations.

SWIR (Short-wave infrared) Hyperspectral images were recorded using HySpex SWIR-384 camera, able to record the specific radiance of materials' surface between 950-2550 nm. The hyperspectral imaging spectrometer simultaneously registered 288 spectral bands. The data were registered using a linear push-broom scanning technique, with a lens for 30 cm distance. Due to the shape of the vessel some areas were out of focus. However, this drawback was minimized by using multiple recordings for the specific areas of interest and by adjusting the distance from the camera to the object. The object was diffusely illuminated with two custom made lamps, which focused the light in a vertical line overlapping with the narrow FOV of 16 degrees across the track. Data processing was carried out with ENVI (Harris Corporation).

Optical microscopy (OM) was performed on some of the samples with Leica M205FA fluorescence stereomicroscope, equipped with PlanApo objective at 52x magnification.

RESULTS AND DISCUSSION

X-Ray imaging

The first radiographs were acquired soon after the excavation, before preliminary cleaning. The results indicated the same type of deposition inside and outside the object. As can be seen in **Fig. 2**, no other objects were identified inside. X-ray imaging revealed that the vessel's walls were thin (~ few millimeters) and fragile, details important for future handling.

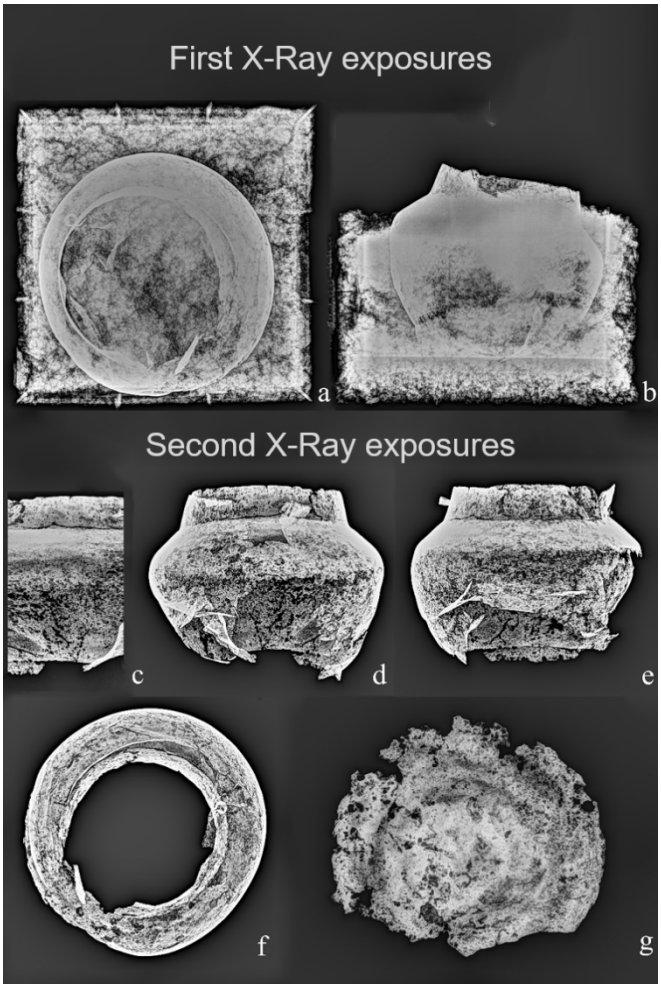

Fig. 2. First X-ray imaging: a) top view; b) side view; X-ray imaging after the preliminary cleaning: c) single wall; d)-e) orthogonal axis views; f) vertical view; g) base fragment (over scaled for better observation).

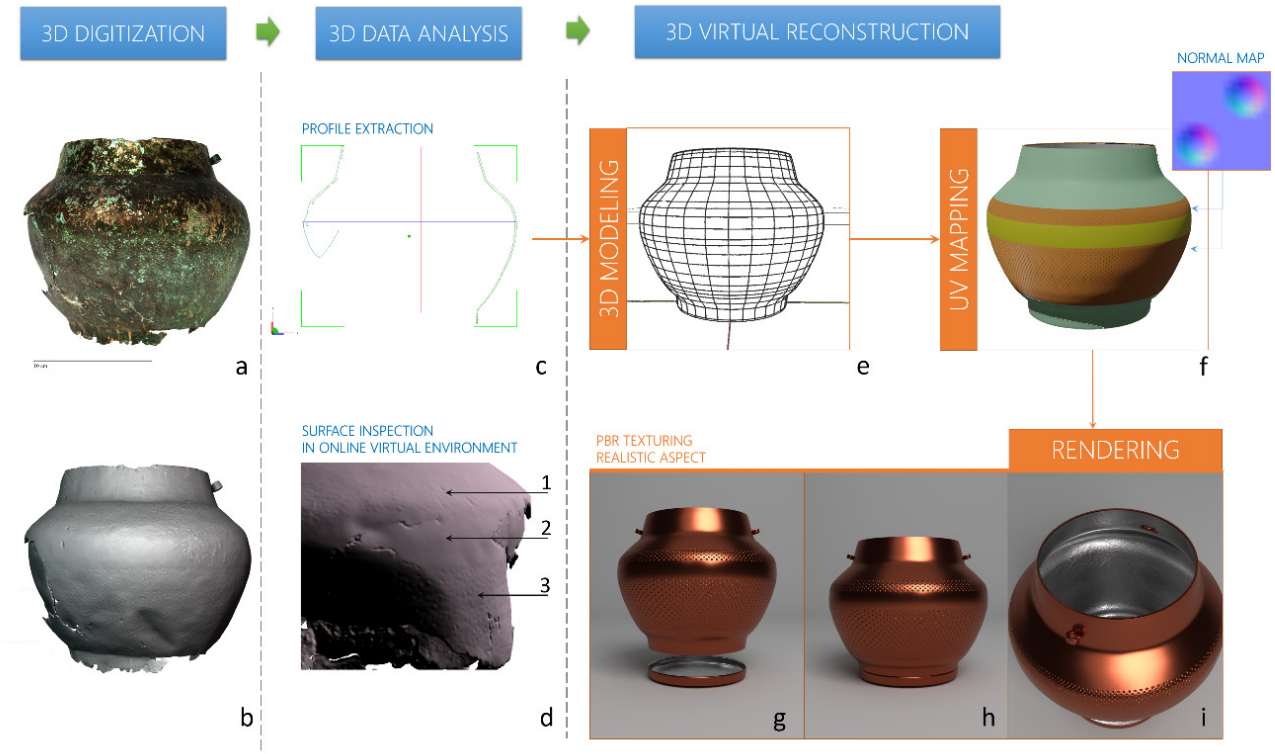

Fig. 3. a) realistic texturing; b) MatCap rendering;) Y axis (green) profile of 3D digitized vessel; d) embossed decorations emphasized by interactive raking light tool, showing the shoulder decoration (area a), the polished median band (area b), the lower register decoration (area c); Stages of the virtual reconstruction: e) hard surface modeling (wireframe view); f) UV mapping of areas with different properties of the object and the normal map; g-i) rendered views of the final reconstruction (Supplementary material 2).

The radiographs from the second exposure session, after the vessel's preliminary cleaning (**Fig. 2c-g**) showed clues to a hypothetic repeated hammering of the base's alloy center, from interior to exterior, following a spiral path (**Fig. 2-g**). For the decorated parts, there was no indication to their manufacturing. **Fig. 2c** shows a side view of the vessel recorded using a flexible film which was inserted inside the vessel, to determine the conservation state of the metal. This way, the superimposition of the vessel walls (as seen in **Fig. 2d-e**) was avoided. Important structural details like the crack along the base of the vessel neck, which was not visible otherwise, were clearly emphasized (**Fig. 2c-e**). This kind of information is essential for the restorers as they can better assess their conservation strategy.

3D digitization and the virtual reconstruction proposal

The photogrammetric processing resulted in a 3D digitized model of the object with 159 million polygons. The resulted mesh was cleaned of any remaining polygon debris and 8182 pixels textures (8k) were generated for both diffuse and normal mapping. In this case the mesh simplification was done at 100.000 polygons for further online usage.

By applying a special type of texture that maps using the surface normal (MatCap - Material Capture) with a Cavity enhancing algorithm (which highlights the valleys and ridges on the surface of the 3D model, thus emphasizing all the smaller details), it was possible to observe in detail the decorations on the lower register of the vessel (**Fig. 3b**). Using this combined visualization, another detail was observed: a well-defined median band of 2.3 cm surrounding the object (**Fig. 3d**, area *2*), where the surface appeared almost polished. From that band below starts the decorated register for about 5.2 cm (**Fig. 3d**, area *3*) and above it for about 1.3 cm another decoration register (**Fig. 3d**, area *1*).

Using an online web visualizer, 3D HOP[22], for easier shared inspection of the 3D model, the decorations on both sides of the median band were emphasized with a raking light interactive tool (**Fig. 3d**).

Based on this reconstruction, precise measurements could be possible: volume, areas, decoration sizes, wall thicknesses anywhere on the body, etc. Also, an important advantage was the extraction of profile on all three axes (**Fig. 3c**), which helped in the comparative studies with other vessels' shape and in the design of the proposed 3D virtual reconstruction.

For virtual reconstruction, the first intent was to realize a virtual anastylosis, but the vessel fragments were too small to be used for this purpose. Therefore, the only digitized piece used was actually the body of the vessel. For modeling purposes, the simplified (100.000 polygons) reconstructed model and the most intact extracted profile shape were used as references (**Fig. 3g-i**). The thickness of the original model varied between 1.77 mm (upper neck area) and 2.37 mm (the widest area), so for the virtual reconstruction we opted for a constant wall thickness of 2 mm. The decorations on the lower half and the shoulder

[22] POTENZIANI *et alii* 2015.

of the object all have 1.8 mm diameter, with an apparent random distribution with a distance between adjacent spots ranging between 0.5 mm and 1.5 mm.

Spectroscopic methods

Firstly, data were collected regarding the corrosion products derived from the original bronze material, and respectively, from the local environment in which the vessel had been buried for almost 2000 years, after which one of the samples (7) has been mechanically cleaned and the concentration of the identified elements was detected for the bulk metal using empirical calibrations for copper. The visual aspect of the samples varied from black, dark green to light blue-green (Supplementary material 1). Some of the samples had a thick layer of soil. In all cases, the surface was highly inhomogeneous and rough, with a soil layer, followed by a black layer, and then a green layer, sometimes interlaced with the black areas. The side view of sample 7 showed an intermediary layer consisting of orange inclusions from the core metal towards the outer layers.

Copper was the main identified element in all XRF spectra, followed by several trace elements, such as Fe, Sn, Pb, Sb, Ag. Even samples covered by a relatively thick soil layer showed Cu as the main element, probably due to microscopic Cu particles embedded in the soil matrix. Tin and lead could have been added in bronzes to make them more fluid and easier to work[23]. Other identified metals and metalloids, such as Fe, Ag, Sb, As which may commonly be found in archaeological bronzes, are usually indicators of either the copper ore used or of the manufacturing process[24]. The surface corrosion layer formed on sample 7 was analyzed by XRD. The main corrosion products found were basic salts and oxides of the main elements found by XRF (Cu, Pb, and Sn): brochantite ($Cu_4(SO_4)(OH)_6$), malachite ($Cu_2(CO_3)(OH)_2$), cerussite ($PbCO_3$), atacamite ($Cu_2Cl(OH)_3$), libethenite ($Cu_2(PO_4)(OH)$), tenorite (CuO), covellite (CuS), cassiterite (SnO_2), pyromorphite ($Pb_5(PO_4)_3Cl$), cuprite (Cu_2O) (**Fig. 4f**).

Brochantite indicates a lesser sulfur concentration in the soil, as it forms from posnjakite, derived from cuprite, as opposed to a higher-sulfur content in the soil, which would have led to the formation of antlerite[25], component not identified in the diffractogram.

Cuprite forms through the oxidation of copper in alkaline soils, and, in contact with carbonates from groundwater, turns into malachite[26]. In chloride-rich conditions, cuprite can turn to nantokite, and then into atacamite, indicator of the so-known "bronze disease"[27]. Malachite was also confirmed via FTIR-ATR spectra of corrosion products, **Fig. 4a** – characteristic peaks at: 1496 and 1392 cm^{-1} (CO stretching), 1097 and 1035 cm^{-1} (CO symmetric and asymmetric stretching vibrations), 818 and 750 cm^{-1} (CO stretching modes), 580, 516 and 427 cm^{-1} (Cu-O skeleton vibrations)[28]. Compared to the reference spectra of malachite, the broad bands in the 3400 cm^{-1} region (OH stretching mode) - peaks at 3442 and 3336 cm^{-1}, are slightly shifted towards higher wavenumbers. This is most probably due to overlapping signal with the different impurities that are present[29]. A green carbonate-based corrosion product, malachite is frequently found on copper-based artifacts that have been exposed to prolonged burial in soil[30]western Iran, was established to identify corrosion morphology and mechanism in these objects. The corrosion layers in 22 samples were studied by optical microscopy, scanning electron microscopy–energy-dispersive X-ray spectroscopy and X-ray diffraction methods. The results showed that a thin corrosion crust has formed on the surface of bronzes with a triple-layer structure, including two internal and one external corrosion layers. The formation of these layers is due to copper leaching from the bronze surface. The internal corrosion part has been a compact, tin-rich corrosion/oxidation product (noble patina.

Broad carbonate stretching bands in the 1400-1500 cm^{-1} region and a hydroxyl function around 3400 cm^{-1} identified in the FTIR spectra suggest the presence of carbonates[31], probably from lead carbonate, as indicated by XRD. XRF showed higher Pb concentration in the corrosion layer, as compared to the bulk metal, correlated with the presence of cerussite, probably due to lead leaching, which may occur in the presence of organic acids[32].

The dull-black tenorite can form from copper slowly heated in air, before or during the burial[33]. Libethenite and pyromorphite, not very frequent copper phosphate corrosion products, are most often encountered in soils rich in phosphorous, either from natural sources (bones, ivory, soil apatite), or from anthropological sources (phosphorous-based fertilizers). In addition, quartz (SiO_2), hematite (Fe_2O_3) and the aluminosilicate halloysite, ($Al_2Si_2O_5(OH)_4$) could be identified in the diffractogram, coming from the soil[34].

Black corrosion products were also investigated by FTIR, showing broad, poorly defined absorption bands at 1555, 1379 and 1031 cm^{-1} (**Fig. 4c**). According to XRF data, several metal oxides could be present. The peak around 1030 cm^{-1} could be linked with the presence of manganese dioxide or of silica content[35]. The peaks at 874 and 712 cm^{-1} are characteristic for calcium carbonate[36]. Calcite should also display a strong absorption around 1400 cm^{-1} (asymmetric stretch), that overlaps in this case with the other present components. The weak bands at 2922 and 2852 cm^{-1} could be ascribed to aliphatic C–H stretch groups. However, as no organic residues were found in any of the investigated samples (including soil), these bands are most probably due to carbonate overtone/combinations[37].

[23] INGO *et alii* 2006; OUDBASHI/MOHAMMADAMIN/DAVAMI 2012.
[24] INGO *et alii* 2006.
[25] KRÄTSCHMER/ODNEVALL WALLINDER/LEYGRAF 2002.
[26] COSANO *et alii* 2018.
[27] CHANG *et alii* 2019; COSANO *et alii* 2018.
[28] ROY 1993; KOTLAR *et alii* 2021.
[29] KOTLAR *et alii* 2021.
[30] OUDBASHI/HASANPOUR/DAVAMI/ 2016; COSANO *et alii* 2018; FAN 2019.
[31] ROY 1993.
[32] SCOTT 2002.
[33] SCOTT 2002.
[34] MANSO *et alii* 2015; OUDBASHI 2018.
[35] BIKIARIS *et alii* 2000.
[36] ROY 1993; KOTLAR *et alii* 2021.
[37] SHILLITO *et alii* 2009.

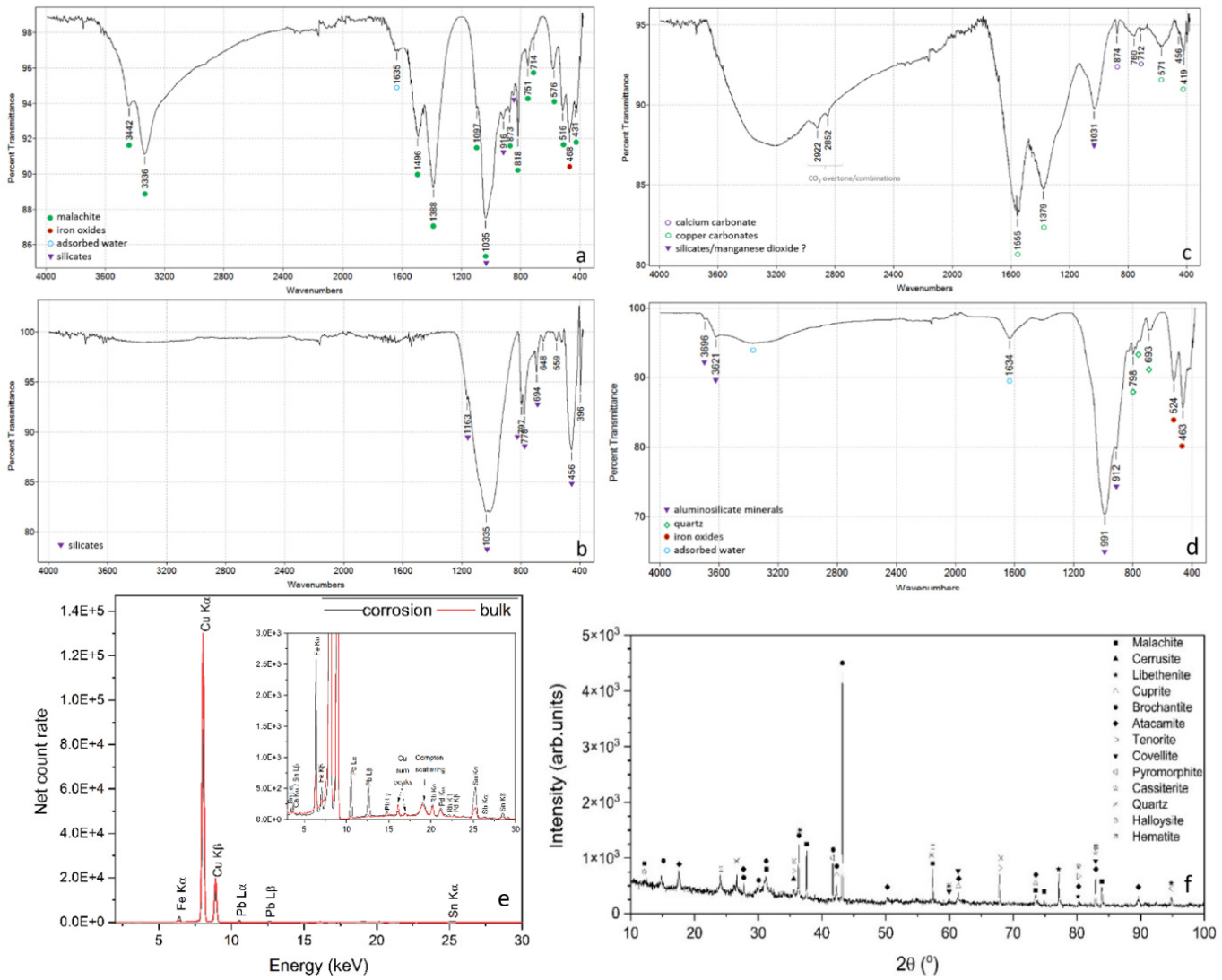

Fig. 4. FTIR-ATR spectra of corrosion products: a) greenish layer; b) orange-red layer; c) black layer; d) sedimentary matrix; e) XRF of sample 7; f) XRD of corrosion from sample 7.

FTIR spectra of the red/orange corrosion products (**Fig. 4b**) indicate a rich silica content – main absorption at 1035 cm^{-1}, sharp peaks at 797 and 778 cm^{-1} due to the asymmetrical and symmetrical stretching vibrations of the Si-O groups, peaks at 694 and 456 cm^{-1} ascribed to Si-O bending vibrations[38]. The band at 695 cm^{-1} is a clear indicator for quartz crystallinity[39]. This high silica content could be linked with the formation of secondary silica[40].

Regarding the bulk material, the normalized XRF intensities of the main identified elements for sample 7 showed that while copper concentration is higher at the core of the sample, the surface corrosion layer is enriched in Fe, Pb, Sn and Sb (**Fig. 4e**). The higher tin content in the external layer would indicate an intercalation of Sn-derived products within copper-based corrosion layers[41]. Similarly, the higher Pb concentration in the corrosion layer can be explained by the preferential mineralization of Pb aggregates in copper matrix[42]. On the other hand, Fe is most likely related to the soil input, which explains its much higher concentration in the corrosion layer as compared to the bulk. For the bulk metal, elemental concentrations were approximately 97 wt% for Cu, 1.18 wt% for Sn, 0.30 wt% for Fe, 0.27 wt % for Pb, 0.15 wt % for Sb, and 0.11 wt% for Ag, which would place the vessel into the low – tin category[43].

Soil samples attached to the artifact were also analyzed by FTIR. As shown in **Fig. 4d**, aluminosilicate minerals were identified via the characteristic absorptions in the upper region of the spectra – peaks at 3696 and 3621 cm^{-1} assigned to OH groups from the Al-OH and Si-OH surface[44], and the shoulder band at 912 cm^{-1} (deformation mode of the Al_2OH group). The 3697 cm^{-1} band is characteristic for kaolinite. However, the main vibration of kaolinite[45], typically centered at 1030 cm^{-1} (SiO deformation mode), with a shoulder band at 1011 cm^{-1} (Si-O-Al), is slightly shifted towards lower wavenumbers – 991 cm^{-1}. This situation could be due to interferences with the 1085 cm^{-1} band in quartz

[38] SAIKIA/PARTHASARATHY/SARMAH 2008.
[39] SAIKIA/PARTHASARATHY/SARMAH 2008.
[40] CRANE/SHARPE/WILLIAMS 2001.
[41] CHANG *et alii* 2020.
[42] INGO *et alii* 2019.
[43] SCOTT 2002.
[44] DONTSOVA *et alii* 2004.
[45] SALAMA/EL AREF/GAUPP 2015.

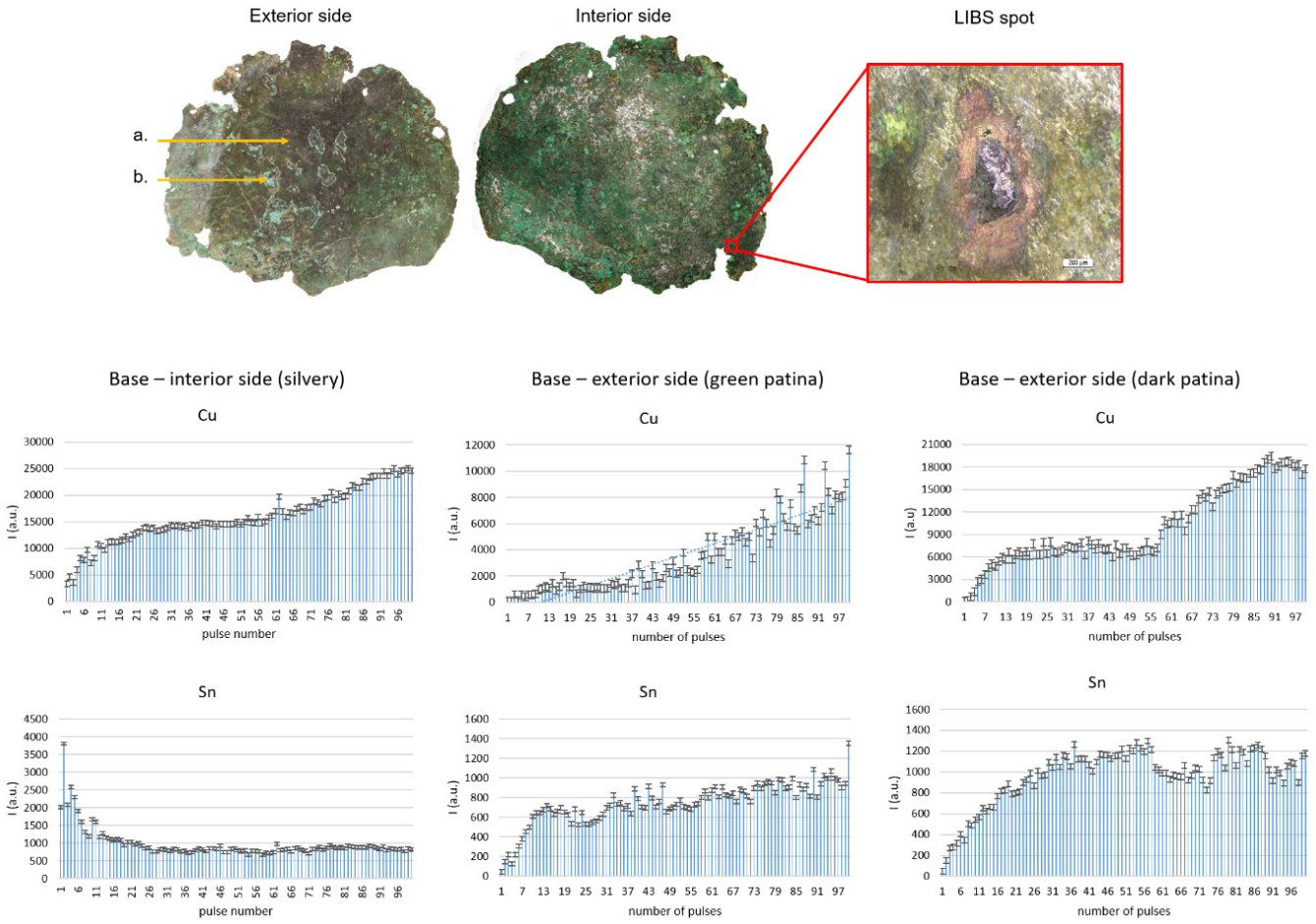

Fig. 5. LIBS analysis areas and stratigraphy data on the interior and exterior side of the base.

(also present), as well as to particle size[46]. Small amounts of quartz could be inferred as indicated by the weak but very characteristic doublet observed at 798 and 778 cm^{-1} (Si-O symmetrical stretching vibration), and the peak at 693 cm^{-1} (Si-O symmetrical bending vibration)[47]. As suggested by XRF, iron is present in the soil matrix, in relatively high amounts, considering the intensity of the characteristic absorption bands at 524 and 463 cm^{-1}, slightly shifted towards lower wavenumbers compared to the reference peaks registered for ferric oxide/mineral hematite[48]. As shown in previous studies, this situation could be explained by an increase of Al- for Fe-substitution in the hematite structure[49]. The small peak around 1634 cm^{-1} (H–O–H bending vibration) with an overtone around 3300 cm^{-1}, can be related to adsorbed water on clay surfaces[50]. No traces of organic materials were found.

The LIBS spectra can give important data about the distribution of the elemental composition on stratigraphy; thus, the Roman vessel and its fragments were investigated using 100 pulses because of the thick crust of surface corrosion and adherent deposits. From all the data processed, several spots were analyzed on some of the samples, but the most important results were obtained on the base (**Fig. 5**), for which a suspicion existed regarding the composition of the interior side.

The stratigraphy investigations were focused on the evaluation of the distribution of Cu, Sn, Pb and Si throughout the LIBS series, taking into consideration the type of adherent deposits present on the surface: dark corrosion, green corrosion and soil adherent deposits. The stratigraphical distribution of Sn shows that it has a higher abundance in the corrosion layer, while Cu concentration begins to increase after the first 25-30 pulses, showing higher abundance in the core of the metal, in accordance with the XRF results. Comparing the green and dark black corrosions, it appears that Cu has a smooth continuous increase for the green corrosion, while for the darker crust, it shows a slight increase, than reaches a plateau and after the 60th pulse it has a greater increase. Si content is, as expected, much higher in the soil crust as compared to the other corroded surfaces.

The base presents areas where the exterior black corrosion is exposing the green layer underneath, therefore the LIBS was performed on both green and dark areas. Due to the fact that both sides of the base presented surface corrosion, the copper signal is lower at the surface and increases towards the core of the object, as shown by the LIBS spectra, in accordance with the XRF data. Also, the interior side of the base showed some silvery areas that were

[46] EKOSSE 2005; UDVARDI *et alii* 2017.
[47] SAIKIA/PARTHASARATHY/SARMAH 2008.
[48] BIKIARIS *et alii* 2000.
[49] SALAMA/EL AREF/GAUPP 2015.
[50] DONTSOVA *et alii* 2004; SALAMA/EL AREF/GAUPP 2015.

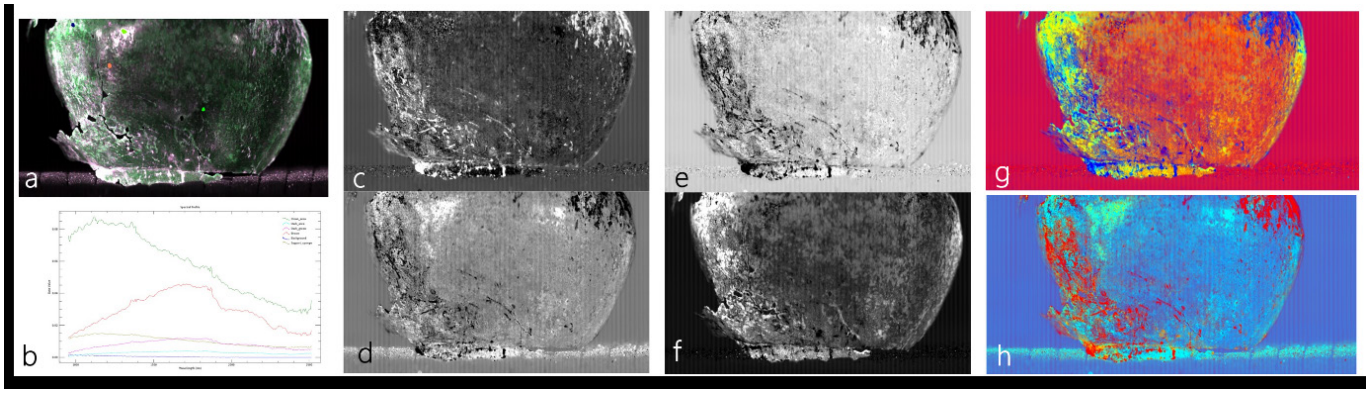

Fig. 6. a) Regions of Interest (ROI); b) spectra corresponding to the ROIs; c-f) LSU algorithm abundance maps for the selected areas: mauve (c), dark (d), shiny (e), light green (f); g-h) RGB combinations: Red – dark, Green – light green, Blue – mauve (g); Red – mauve, Green – shiny, Blue – dark (h).

also investigated using LIBS stratigraphy. For interior, LIBS stratigraphy data (**Fig. 5**) show a higher relative abundance of Sn in the first pulses that decreases as the pulses advance in the core of the object, as opposed to the exterior which showed a slight increase of tin as pulses advanced. Lead showed similar trend with tin, which proves that there was a Sn+Pb layer applied in the interior of the bronze vessel. The highest intensities were recorded for the second pulse, due to the depositions on the surface layer. As the ablation pulses progress, it can be seen that the bronze material was reached pretty fast, and the Sn and Pb reach a linear area. The presence of Sn on the interior indicates a tin coating, which is specific for storage vessels (used in contact with food, wine or water), excluding its functionality as a cooking vessel, in contact with direct fire or extreme heat[51].

Hyperspectral imaging abundance maps

Hyperspectral data were processed using Linear Spectral Unmixing (LSU) algorithm, to obtain abundance maps[52]. Using different RGB values combinations, variability of the spectral profiles was highlighted in False Color Infrared (FCIR) images. Using vector layers converted into *Region of Interest* (ROI) areas (**Fig. 6a**) endmembers were collected for the categories that had a characteristic response of the spectra, in terms of radiance value and wavelength. For each of these categories the mean value of the spectral profiles found in the ROI selections was exported as statistic files. This data was actually used in the process of calculation as endmembers to determine the relative abundance of the compounds (mapped as raster images together with the Root Mean Square error).

In **Fig. 6c-f**, the light and dark areas designate high, respectively low, pixel purity/accuracy matches. The fraction corresponding to the darker areas in **Fig. 6a**, covering most of the vessel, is linked to the surface depositions, which showed greater absorbance in the NIR as compared to the visible. Light green and mauve fractions have well individualized spectra, their highest purity signal being located in different areas than the darker depositions. The fraction corresponding to the shiny areas represents a particular case. Due to its appearance in FCIR images and slightly different spectral profile we have considered this area to be individualized but taking in consideration the overall output data it can be understood as a mismatch selection when looking at the fractions of light green and dark depositions. A better understanding of the distribution of pixel purities' abundances has been reached using their combinations in RGB as seen in **Fig. 6g-h**. Although the intensity of the signal was very low due to the surface depositions, the mixing calculation based on the least-squares inversion method was able to discriminate the main categories of materials.

The LSU maps showed how the various degradation compounds are mixed at and below the surface of the object. These maps can aid the restoration process, guiding the restorer to apply the proper cleaning procedures even in areas where corrosion layers overlap.

CONCLUSIONS

The Roman vessel analyzed in this study is an uncommon discovery in many ways. Only a few bronze vessels with a globular shape, small size and embossed dotted decoration were found in other museum collections, unavailable to the public, but with significant differences. Unfortunately, there were no scientific investigations carried out for them, hence the importance of the present study. The historical context of the Mălăiești fort leads to a precise dating (101 – 118 A.D.) of the object, placing it in the same time frame with the referenced vessels.

The opportunity of documenting the vessel, through a multi-analytical integrated approach right after its discovery was a great advantage for its characterization, especially for studying the corrosion and overall conservation state.

The X-ray imaging emphasized the content of the vessel after the first exposure, ruling out the possibility of other objects being hidden in the soil inside the vessel, useful for the first mechanical cleaning of the vessel. The second exposure, after the cleaning, was helpful in identifying traces specific for the manufacturing process (such as the hammering process for the base), along with the assessment of the vessel's state of degradation – wall thickness, integrity and heterogeneity.

[51] MUSTAȚĂ 2017.
[52] CANTY 2014; DEBORAH/ULFARSSON/SIGURDSSON 2021; GRILLINI/THOMAS/GEORGE 2021.

3D digitization is an important stage in both structural and visual documentation of any artefact. From the 3D digitized model were extracted precise measurements regarding wall thickness all across the vessel surface (ranging between 1.77 and 2.37 mm), decoration and other small detail sizes, shape profiles and, finally, it was the direct reference for the virtual 3D reconstruction. The virtual reconstruction aimed at an ideal shape and form of the vessel, as it is supposed to have been when it was anew. The only loop preserved on the edge of vessel indicated that it probably had a handle, but with no clues regarding the shape and the construction technique. Therefore, the reconstruction did not include any handle hypothesis. The PBR texturing was used in order to give a real-life look with real metal properties (the way it interacts with light). The color chosen was estimated in accordance with the results of the XRF characterization, which indicated a Cu-Sn alloy (97 wt% for Cu, 1.18 wt% for Sn).

The resulted 3D model can be viewed in an online web browser[53], but it can also be used in a physical exhibition along with the original object, in digital form (animation, interactive 3D model) or in physical form (digital prints, 3D print). Such renderings, based on and associated with accurate analytical data, can be useful in enriching the museum display of objects and could be well received by the public, which could gain a more realistic perception on how the object would have originally looked like. The virtual reconstruction has uses beyond the online edutainment sphere, as it can bring added value for a better understanding of the typology and the use of the vessel.

The X-ray diffraction analysis, along with the spectroscopic characterization, indicated the presence of several degradation compounds of the main elements, such as brochantite, malachite, cerussite, cuprite, atacamite, cassiterite, covellite, tenorite, pyromorphite and libethenite. Some of these compounds can give indications about the features of the surrounding soil: the phosphates, in the lack of any other specific indicators, point towards agricultural practices, copper oxide might suggest the presence of groundwater sources, while brochantite infers a low-sulfur content in the soil, which is consistent with soil leaching as a result of precipitation or how much water is running through the soil profile, either from groundwater sources or from watering of the crops. Infrared spectroscopy highlighted the presence of typical soil components, such as quartz, aluminosilicate minerals (kaolinite) and iron oxides, without any traces of organic materials. All of these together indicate a specific fingerprint left upon the object by the characteristic features of the burial area, where the soil was cultivated, fertilized, and frequently watered.

LIBS stratigraphical analysis allowed a high accuracy comparison between the surface corrosion layers and the bulk, with higher Cu concentration towards the interior, as compared to the outside of the samples. An important aspect was the detection of higher Sn and Pb concentration in the first spectra for the measurements performed on the silvery areas on the interior of the base.

[53] ANGHELUTA *et alii* 2022.

Since neither the FTIR nor the GC-MS (inconclusive data, not included in this paper) performed on the soil taken from inside of the vessel yielded any traces of organics, there is no assumption as to what it may have contained. However, the discovery of tin coating on the inside of the vessel narrows down its possible uses, indicating that it was most probably used for storage of food or liquids, but not for cooking, nor in contact with direct fire or extreme heat.

Knowing the precise dating of the archaeological site, and thus of the object, and also the results of this integrated multi-analytical approach, the object can become a reference for future studies regarding bronze artifacts found in similar forts, not only from the Dacian territory but also from the neighboring region.

ACKNOWLEDGEMENTS

This study was financed by the Ministry of Research and Innovation through "Program Nucleu" PN 19-18.01.01: OPTRONICA VI.

The authors are grateful to Dr. Silvia Mustață, from the Ancient History and Archaeology Department of the Faculty of History and Philosophy, Babeș-Bolyai University in Cluj, Romania, for her contribution in understanding the typology and use of the vessel, and to Alexandru Dozsa from the National Museum of Romanian History, in charge of the vessel's restoration. Special thanks for curator Jasper de Bruin from the Rijksmuseum van Oudheden, Leiden, Netherlands, for providing information regarding the Leiden vessel.

REFERENCES

AGRESTI *ET ALII* 2016

Agresti, J./Osticioli, I./Guidotti, M.C./Kardjilov, N./Siano, S., Non-invasive archaeometallurgical approach to the investigations of bronze figurines using neutron, laser, and X-ray techniques, *Microchemical Journal*. DOI: 10.1016/j.microc.2015.10.030.

ALBERGHINA *et alii* 2011

Alberghina, M. F./Barraco, R./Brai, M./Schillaci, T./Tranchina, L., Integrated analytical methodologies for the study of corrosion processes in archaeological bronzes, *Spectrochimica Acta - Part B Atomic Spectroscopy*. DOI: 10.1016/j.sab.2010.12.010.

ANGELINI *et alii* 2004

Angelini, E./Mongiatti, A./Grassini, S./Rosalbino, F./Ingo, G. M./De Caro, T., Comparative study of the corrosion process of buried Italian bronze artefacts and of aged copper-based alloys of similar composition, in EUROCORR 2004 - European Corrosion Conference: Long Term Prediction and Modelling of Corrosion.

ANGHELUTA 2019

Angheluta, L., *Practical guide and applications of photogrammetry in cultural heritage 3D digitization* (Cluj-Napoca: Mega Publishing House).

ANGHELUTA *et alii* 2022

Angheluță, L., Țentea, O. Dozsa, AL. Virtual reconstruction and restoration of an uncommon bronze vessel from the Mălăiești Roman fort, Cercetări Arheologice 29.1, 2022. DOI: https://doi.org/10.46535/ca.29.1.12

BARATTE *et alii* 1984

Baratte, F./Bonnamour, L./Guillaumet, J.-P./Tassinari, S., *Vases antiques de métal au Musée de Chalon-sur-Saône* (Revue arch. Dijon).

BIKIARIS *ET ALII* 2000

Bikiaris, D./Daniilia, Sister/Sotiropoulou, S./Katsimbiri, O./Pavlidou, E./Moutsatsou, A. P./Chryssoulakis, Y., Ochre-differentiation through micro-Raman and micro-FTIR spectroscopies: Application on wall paintings at Meteora and Mount Athos, Greece, *Spectrochimica Acta - Part A: Molecular and Biomolecular Spectroscopy*. DOI: 10.1016/S1386-1425(99)00134-1.

CANTY 2014

Canty, M. J., Image analysis, classification and change detection in remote sensing: With algorithms for ENVI/IDL and python, third edition. DOI: 10.1201/b17074.

CHANG *et alii* 2019

Chang, T./Herting, G./Goidanich, S./Sánchez Amaya, J. M./Arenas, M. A./Le Bozec, N./Jin, Y./Leygraf, C./Odnevall Wallinder, I./The role of Sn on the long-term atmospheric corrosion of binary Cu-Sn bronze alloys in architecture, Corrosion Science. DOI: 10.1016/j.corsci.2019.01.002.

CHANG *et alii* 2020

Chang, T./Maltseva, A./Volovitch, P./Odnevall Wallinder, I./Leygraf, C., A mechanistic study of stratified patina evolution on Sn-bronze in chloride-rich atmospheres, *Corrosion Science*. DOI: 10.1016/j.corsci.2020.108477.

CHELMUS/RADVAN/GHERVASE 2018

Chelmus, A./Radvan, R./Ghervase, L., Corroborated X-ray imaging and elemental analysis for obtaining quantitative information from radiographs, *Optoelectronics and Advanced Materials, Rapid Communications* 12 (5-6), 314-318.

COSANO *et alii* 2018

Cosano, D./Esquivel, D./Mateos, L.D./Quesada, F./Jiménez-Sanchidrián, C./Ruiz, J.R., Spectroscopic analysis of corrosion products in a bronze cauldron from the Late Iberian Iron Age, *Spectrochimica Acta - Part A: Molecular and Biomolecular Spectroscopy*. DOI: 10.1016/j.saa.2018.07.072.

CRANE/SHARPE/WILLIAMS/2001

Crane, M. J./Sharpe, J. L./Williams, P. A., Formation of chrysocolla and secondary copper phosphates in the highly weathered supergene zones of some Australian deposits, Records of the Australian Museum. DOI: 10.3853/j.0067-1975.53.2001.1323.

DEBORAH/ULFARSSON/SIGURDSSON/2021

Deborah, H./Ulfarsson, M.O./Sigurdsson, J., Fully Constrained Least Squares Linear Spectral Unmixing of The Scream (Verso, 1893), 2021 11th Workshop on Hyperspectral Imaging and Signal Processing: Evolution in Remote Sensing (WHISPERS), 1–5. DOI: 10.1109/WHISPERS52202.2021.9484037.

DONTSOVA *et alii* 2004

Dontsova, K. M./Norton, L. D./Johnston, C.T./Bigham, J. M., Influence of Exchangeable Cations on Water Adsorption by Soil Clays, Soil Science Society of America Journal. DOI: 10.2136/sssaj2004.1218.

EKOSSE 2005

Ekosse, G.-I. E. Fourier transform infrared spectrophotometry and X-ray powder diffractometry as complementary techniques in characterizing clay size fraction of kaolin, *Journal of Applied Sciences and Environmental Management*. DOI: 10.4314/jasem.v9i2.17289.

FACSÁDY/VEREBES 2009

Facsády, A. R./Verebes, A., Analysis of roman bronze finger rings from aquincum, *Materials and Manufacturing Processes* 24(9), 993–998. DOI: 10.1080/10426910902979942.

FAN 2019

Fan, X. Characteristics of mimetite(Pb5(AsO4)3Cl)-pyromorphite(Pb5(PO4)3Cl) corrosion products on Han Dynasty bronzes from Chongqing, China, *Microchemical Journal*. DOI: 10.1016/j.microc.2019.104062.

GRAZZI *et alii* 2019

Grazzi, F./Cucci, C./Casini, A./Stefani, L./Kardjilov, N./Thiele, A./Hošek, J./Picollo, M., Merging of imaging techniques based on reflectance hyperspectral and neutron tomography for characterization of a modern replica of a 13th century knife from Croatia, 11058, 1105816. DOI: 10.1117/12.2526050.

GRILLINI/THOMAS/GEORGE/2021

Grillini, F./Thomas, J.-B./George, S., Comparison of Imaging Models for Spectral Unmixing in Oil Painting, *Sensors* 21(7), 2471. DOI: 10.3390/S21072471.

HODGSON/BIDWELL 2004

Hodgson, N./Bidwell, P. T., Auxiliary Barracks in a New Light: Recent Discoveries on Hadrian's Wall, *Britannia* 35, 121–157.

INGO *et alii* 2006

Ingo, G. M./De Caro, T./Riccucci, C./Angelini, E./Grassini, S./Balbi, S./Bernardini, P./Salvi, D./Bousselmi, L./Çilingiroğlu, A./Gener, M./Gouda, V. K./Jarrah, O. A.L./Khosroff, S./Mahdjoub, Z./Saad, Z. A.L./El-Saddik, W./Vassiliou, P., Large scale investigation of chemical composition, structure and corrosion mechanism of bronze archeological artefacts from Mediterranean basin, *Applied Physics A: Materials Science and Processing*. DOI: 10.1007/s00339-006-3550-z.

INGO *et alii* 2019

Ingo, G. M./Riccucci, C./Guida, G./Albini, M./Giuliani, C./Di Carlo, G., Rebuilding of the Burial Environment from the Chemical Biography of Archeological Copper-Based Artifacts, *ACS Omega*. DOI: 10.1021/acsomega.9b00569.

KOSTER/RIEDERER 1997

Koster, A./Riederer, J. *The bronze vessels 2. Acquisitions 1954-1996* (Nijmegen: Provincie Gelderland, Provinciaal Museum).

KOTLAR *et alii* 2021

Kotlar, M./Matijaković Mlinarić, N./Desnica, V./Marušić, K., Studying a 2 millennia old bronze kettle using easily accessible characterization techniques, *Heritage Science*. DOI: 10.1186/s40494-021-00484-6.

KRÄTSCHMER/ODNEVALL WALLINDER/LEYGRAF/2002

Krätschmer, A./Odnevall Wallinder, I./Leygraf, C., The evolution of outdoor copper patina, *Corrosion Science*. DOI: 10.1016/S0010-938X(01)00081-6.

LIANG 2011

Liang, H. Advances in multispectral and hyperspectral imaging for archaeology and art conservation, *Applied*

Physics A 2011 106(2), 309–323. DOI: 10.1007/S00339-011-6689-1.

MANSO *et alii* 2015

Manso, M./Schiavon, N./Queralt, I./Arruda, A. M./Sampaio, J. M./Brunetti, A., Alloy characterization of a 7th Century BC archeological bronze vase - Overcoming patina constraints using Monte Carlo simulations, *Spectrochimica Acta - Part B Atomic Spectroscopy*. DOI: 10.1016/j.sab.2015.03.001.

MUSTAȚĂ 2017

Mustață, S., *The Roman metal vessels from Dacia Porolissensis* (Cluj-Napoca: Mega Publishing House).

NEVIN/SPOTO/ANGLOS 2012

Nevin, A./Spoto, G./Anglos, D., Laser spectroscopies for elemental and molecular analysis in art and archaeology, *Applied Physics A: Materials Science and Processing*. DOI: 10.1007/s00339-011-6699-z.

NICOLAE *ET ALII* 2014

Nicolae, C./Nocerino, E./Menna, F./Remondino, F., Photogrammetry applied to problematic artefacts, International Archives of the Photogrammetry, Remote Sensing and Spatial Information Sciences - ISPRS Archives, 40(5), 451–456. DOI: 10.5194/isprsarchives-XL-5-451-2014.

OPAIȚ 2017

Opaiț, A., On the local production and imports of wine in the Pontic and Lower Danube regions (1st century BC to 7th century AD). An overview. In: Dixneuf, D. (ed.), Late Roman coarse wares, cooking wares and amphorae in the Mediterranean. Archaeology and archaeometry. La céramique commune, la céramique culinaire et les amphores de l'Antiquité tardive en Méditerranée. *Archéologie et archéométrie* 2, 581–587.

OUDBASHI 2018

Oudbashi, O., A methodological approach to estimate soil corrosivity for archaeological copper alloy artefacts, *Heritage Science*. DOI: 10.1186/s40494-018-0167-4.

OUDBASHI *et alii* 2012

Oudbashi, O./Mohammadamin, S./Davami, P., Bronze in Archaeology: A Review of the Archaeometallurgy of Bronze in Ancient Iran. In: Collini, L. (ed.), *Copper Alloys - Early Applications and Current Performance - Enhancing Processes*. DOI: 10.5772/32687.

OUDBASHI *et alii* 2016

Oudbashi, O./Hasanpour, A./Davami, P. Investigation on corrosion stratigraphy and morphology in some Iron Age bronze alloys vessels by OM, XRD and SEM–EDS methods, *Applied Physics A: Materials Science and Processing*. DOI: 10.1007/s00339-016-9793-4.

POTENZIANI *et alii* 2015

Potenziani, M./Nocerino, E./Menna, F./Remondino, F., 3DHOP: 3D Heritage Online Presenter, *Computers and Graphics (Pergamon)* 52, 129–141. DOI: 10.1016/j.cag.2015.07.001.

REMONDINO 2011

Remondino, F. Heritage recording and 3D modeling with photogrammetry and 3D scanning, *Remote Sensin* 3(6), 1104–1138. DOI: 10.3390/rs3061104.

ROY 1993

Roy, A. (ed.), *Artists' Pigments. A Handbook of Their History and Characteristics*, Vol. 2. (Washington: National Gallery of Art).

RUBIO-BARBERÁ *et alii* 2019

Rubio-Barberá, S./Fragoso, J./Gallello, G./Arasa, F./Lezzerini, M./Hernández, E./Pastor, A./de la Guardia, M., Analysis of Sagunto Ibero-Roman votive bronze statuettes by portable X-ray fluorescence, *Radiation Physics and Chemistry*. DOI: 10.1016/j.radphyschem.2019.02.031.

SAIKIA/PARTHASARATHY/SARMAH/2008

Saikia, B. J./Parthasarathy/G./Sarmah, N. C./Fourier transform infrared spectroscopic estimation of crystallinity in SiO2 based rocks, *Bulletin of Materials Science* 31(5), 775–779. DOI: 10.1007/s12034-008-0123-0.

SALAMA/EL AREF/GAUPP/2015

Salama, W./El Aref, M./Gaupp, R., Spectroscopic characterization of iron ores formed in different geological environments using FTIR, XPS, Mössbauer spectroscopy and thermoanalyses, *Spectrochimica Acta - Part A: Molecular and Biomolecular Spectroscopy*. DOI: 10.1016/j.saa.2014.10.090.

SCOTT 2002

Scott, D., *Copper and Bronze in Art: Corrosion, Colorants, Conservation* (Los Angeles: The Getty Conservation Institute).

SHILLITO *et alii* 2009

Shillito, L. M./Almond, M. J./Wicks, K./Marshall, L.J. R./Matthews, W., The use of FT-IR as a screening technique for organic residue analysis of archaeological samples, *Spectrochimica Acta - Part A: Molecular and Biomolecular Spectroscopy*. DOI: 10.1016/j.saa.2008.08.016.

ȚENTEA 2018

Țentea, O., Baths and bathing in Dacia during Trajan. In: Sommer, S. C./Matešic´, S. (eds.), *LIMES XXIII: Proceedings of the 23rd Congress on Roman Frontier Studies Ingolstadt 2015, Akten des 23. Internationalen Limeskongresses in Ingolstadt 2015*, 4/1 (Mainz : Nünnerich-Asmus Verlag), 133-137.

ȚENTEA/CĂLINA 2019

Țentea, O./Călina, V., Peisajul arheologic al castrului Mălăiești, *Cercetări Arheologice* 26/1, 169–196.

ȚENTEA/MATEI-POPESCU 2015

Țentea, O./Matei-Popescu, F., Why there? The preliminaries of constructing the roman frontier in south-east Dacia, *Acta Musei Napocensis* 52/1, 109–130.

ȚENTEA/POPA/CÎMPEANU 2018

Țentea, O./Popa, A. G./Cîmpeanu, A., Mălăiești. A trajanic fort in Muntenia – the results of recent magnetometric surveys, *Acta Musei Napocensis* 55/1, 227–240.

TUCKER 2012

Tucker, C., Two Roman Bronze vessels from St Nicholas at Wade, Isle of Thanet, *Arcaheologia Cantiana* 132 (223382), 189–214.

UDVARDI *et alii* 2017

Udvardi, B./Kovács, I. J./Fancsik, T./Kónya, P./Bátori, M./Stercel, F./Falus, G./Szalai, Z., Effects of Particle Size on the Attenuated Total Reflection Spectrum of Minerals, *Applied Spectroscopy*. DOI: 10.1177/0003702816670914.

UVAROV/POPOV/ROZENBERG 2015

Uvarov, V./Popov, I./Rozenberg, S., X-ray diffraction and SEM Investigation of Wall Paintings Found in the Roman Temple Complex at Horvat Omrit, Israel, *Archaeometry*. DOI: 10.1111/arcm.12124.

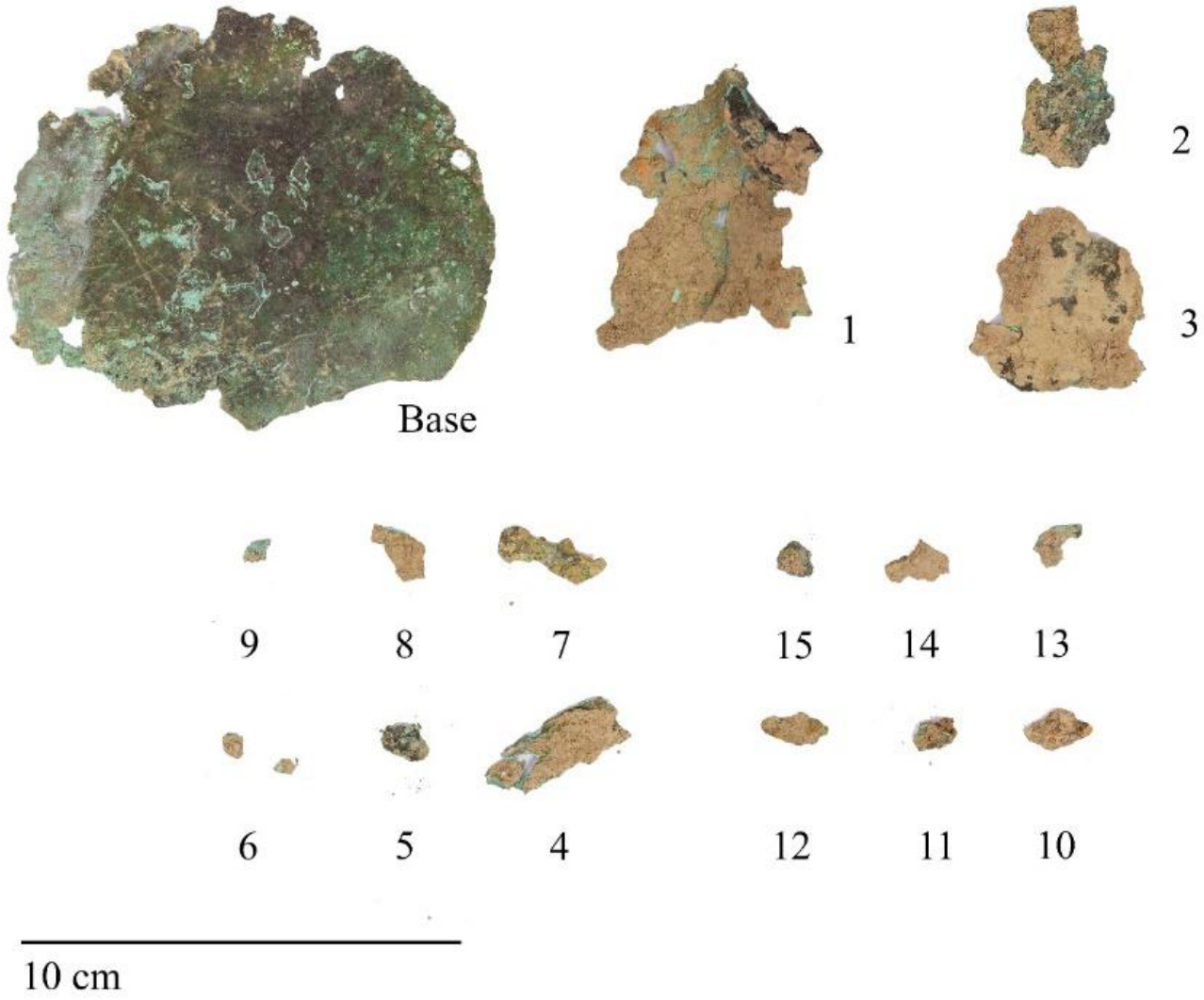

Vessel fragments used as samples in the physico-chemical characterization